Construction and Building Materials 342 (2022) 128013

Contents lists available at ScienceDirect

Construction and Building Materials

journal homepage: www.elsevier.com/locate/conbuildmat

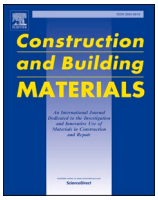

Off-spec fly ash-based lightweight aggregate properties and their influence on the fresh, mechanical, and hydration properties of lightweight concrete: A comparative study

Mohammad Balapour [a,b,*], Mohammad H. Khaneghahi [a], Edward J. Garboczi [c], Yick G. Hsuan [a], Diana E. Hun [d], Yaghoob Farnam [a]

[a] Drexel University, Department of Civil, Architectural and Environmental Engineering, Philadelphia, PA 19104, United States
[b] SusMaX LLC, Philadelphia, PA 19104, United States
[c] National Institute of Standards and Technology, Applied Chemicals and Materials Division, Boulder, CO 80305, United States
[d] Buildings and Transportation Science Division, Oak Ridge National Laboratory, Oak Ridge, TN 37831, United States

ARTICLE INFO

Keywords:
Waste fly ash
Lightweight aggregate
Pore size distribution
Lightweight concrete
X-ray computed tomography
SPoRA

ABSTRACT

An off-spec fly ash-based spherical lightweight aggregate (LWA), designated as Spherical Porous Reactive Aggregate (SPoRA), was manufactured through a lab pilot-scale production and its engineering properties, including specific gravity, dry rodded unit weight, water absorption, mechanical performance, and pore structure, were evaluated. Using SPoRA, lightweight concrete (LWC) samples were made and their fresh, mechanical, and hydration properties were assessed and compared with LWC samples made using two commercial LWA available in the US market. The results indicated that fine and coarse SPoRA had 72 h water absorption capacities of 16.4 % and 20.9 %, respectively, which were higher than that of the two commercial LWAs. Higher saturated surface dry specific gravity of SPoRA compared to commercial LWAs led to a higher fresh density for the corresponding LWC. Using X-ray computed tomography, large spherical type pores were observed in SPoRA similar to those in the commercial slate-based LWA. The pore size distribution of SPoRA, characterized by a dynamic vapor sorption analyzer, indicated that more than 97 % of the pores had diameters greater than 50 nm. SPoRA's average bulk crushing strength was 6.8 MPa which was smaller than commercial LWA and was potentially attributed to the differences in manufacturing processes. Nonetheless, SPoRA LWC with 28 days compressive strength of 29 MPa passed the ASTM C330 requirement and had a comparable strength with LWC prepared with the commercial LWAs indicating lesser importance for the LWA strength. SPoRA LWC had a flowability of 5 % compared to LWC prepared with commercial LWAs having flowability of $\geq$ 18 %. This observation was potentially related to the fluxing agent used in the SPoRA production. SPoRA had a 70 % degree of hydration at 12 days which was comparable with that of LWC prepared with commercial LWA.

1. Introduction

Lightweight aggregate (LWA) can be divided into two categories: (i) natural and (ii) synthetic LWA [1]. Natural LWA (e.g., pumice [2], scoria [3]) are usually formed when molten lava from a volcano cools down leading to the formation of a well-sintered porous microstructure. On the other hand, synthetic LWA are produced by artificial sintering, which can be divided into three categories: (a) natural materials (e.g., clay [4], slate [5], and shale [6]), (b) residential and commercial waste products (e.g., glass [7]), and (c) industrial waste products (e.g., bottom ash [8,9], fly ash [10], sewage sludge [4]). In the U.S., LWA production for use in concrete is mostly focused on sintering natural materials such as clay, shale, and slate. LWA produced from waste products has only a small market share [11,12]. The main reason that industrial waste products like waste fly ash and bottom ash are not used much for LWA production is related to manufacturing technical hurdles for consistent high-quality production.

Fly ash is one of the by-products of burning coal in power plants for electricity production. One of the main applications of fly ash is its use in concrete as a supplementary cementitious material (SCM) for increasing mechanical and durability properties [13]; in this case, it is called in-spec fly ash. However, not all the fly ash produced in the US is

* Corresponding author.

https://doi.org/10.1016/j.conbuildmat.2022.128013
Received 20 February 2022; Received in revised form 26 May 2022; Accepted 30 May 2022

suitable for concrete applications due to its non-compliance with the required specifications found in standards such as ASTM C618 [14] and AASHTO M 295 [15]; this kind of fly ash is called off-spec fly ash. In 2019, nearly 30 million tons of fly ash were generated in the US, of which only 60 % by mass was recycled and the rest (i.e., off-spec fly ash) was disposed to landfills and surface impoundments as industrial waste products [16]. The historical accumulation of unrecycled fly ash can cause damage to the surface water and groundwater, environment, and human health [17,18].

Previous studies have shown that fly ash is in fact an appropriate feedstock material for LWA production [19–22]. However, these studies have mainly focused on using in-spec fly ash for LWA production [23–25]. However, there have been reports of in-spec fly ash shortages for concrete applications in the US [26,27]. As such, researchers have attempted to use **off-spec fly ash** as feedstock material to produce LWA [28]. One of the challenges that has prevented US industrial production of off-spec fly ash-based LWA has been the high variability in the chemical composition of off-spec fly ash [29]. The chemical composition of off-spec fly ash can change dramatically from one landfill to another, which complicates the production of consistent high-quality LWA from this material at an industrial scale. Balapour et al. [9,30] developed a thermodynamics-guided framework that can withstand any changes in the chemical composition of waste bottom ash and fly ash materials and successfully produce LWA from these materials. This thermodynamics-guided framework quantifies the three required conditions including: (i) partial formation of a liquid phase [12,31,32], (ii) appropriate viscosity for solid–liquid phase [33,34], and (iii) formation of gaseous products that are entrapped by the liquid phase to successfully create a porous functional LWA [35,36]. Based on these conditions, the appropriate ranges of temperature and viscosity to successfully produce porous LWA were identified [9].

The main goal of this study is to evaluate whether the thermodynamics-guided framework previously developed by the authors [9] can be successfully used to make, at the scaled-up manufacturing level used as a model for an industrial manufacturing process, off-spec fly ash-based LWA for concrete applications. This study has two main objectives: (1) to characterize the engineering properties and pore structure of scaled-up off-spec fly ash-based LWA and compare it with commercial LWA available in the US market, and (2) to assess the fresh, mechanical, and hydration properties of lightweight concrete (LWC) produced using off-spec fly ash-based LWA and compare it with properties of a LWC made with the same commercial LWA.

2. Experimental program

Table 1 shows the experimental program designed for this study. To address objective #1, physical properties such as specific gravity, dry-rodded unit weight, and water absorption, were measured. Using a dynamic vapor sorption analyzer (DVSA), water desorption behavior was evaluated and its pore structure at the nano scale was characterized. In addition, X-ray computed tomography (XCT) was used to characterize and visualize the pore structure of LWA at the micro scale. The mechanical performance of bulk LWA was also evaluated. To address objective #2, properties including fresh density, workability, and compressive strength of LWC manufactured using off-spec fly ash-based LWA and commercial LWA were assessed. Thermogravimetric analysis (TGA) and isothermal calorimetry methods were used to characterize the phase development and degree of hydration of LWC. The objectives, associated tests, sample type, and purpose of performing each test can be seen in Table 1.

Table 1
Experimental program.

Objective	Test	Sample	Purpose
1	Dynamic Vapor Sorption Analyzer	LWA	To characterize the desorption behavior of LWA and its pore structure at nano scale
	X-ray computed tomography	LWA	To characterize the pore structure of LWA at micro scale
	Crushing resistance	LWA	To assess the mechanical performance of LWA
2	Workability and fresh density	Fresh LWC	To evaluate the fresh properties of LWC
	Compressive strength	Hardened LWC	To evaluate the mechanical performance of LWC
	Thermogravimetric Analysis	Hardened LWC powder	To assess the phase development in LWC
	Isothermal Calorimetry	Mortar	To assess the degree of hydration

2.1. Materials

In this study, one synthetized off-spec fly ash-based LWA along with two commercial synthetic LWAs manufactured from shale and slate were used to produce concrete samples in order to investigate the effect of aggregate properties on the fresh, mechanical, and hydration properties of concrete. In the following section, the manufacturing process of off-spec fly ash-based LWA and the physical properties of LWA is discussed first.

2.1.1. Off-spec fly ash based lightweight aggregate manufacturing

The synthesized off-spec fly ash-based lightweight aggregate, which is denoted as Spherical Porous Reactive Aggregate (SPoRA), was produced by using off-spec high-calcium content fly ash whose chemical composition is reported in Table 2. This fly ash was off-spec because of non-compliance with the ASTM C618 standard. According to this standard, if the fly ash is to be used in concrete, it must have an LOI (loss on ignition) of less than 6 % by mass. However, as can be seen in Table 2, the LOI content for this fly ash was 8.47 %.

The SPoRA manufacturing process includes mixing, pelletization, curing, and sintering. In the mixing stage, dried fly ash powder was mixed with NaOH aqueous solution with a molarity of 2.5 mol/L with a liquid to solid (L/S) mass ratio of 0.2, which led to mass concentrations (i.e., the mass of solid NaOH per mass of solid fly ash) of 2 %. NaOH was used as a fluxing agent to lower the melting temperature of the solid. In addition, NaOH was used for the purpose of initiating geopolymerization in the pelletization stage in order to chemically bind ashes into a spherical shape. The NaOH and L/S ratio have been obtained by optimization based on the previously developed thermodynamics-guided framework [8–10]. A vacuum mixer was used for the mixing process, according to the following procedure: (i) dried fly ash and NaOH solution was first mixed manually for 30 s, (ii) then mixed for one minute at a speed of 2500 RPM (revolutions per minute) using the vacuum mixer, and (iii) steps (i) and (ii) were repeated two

Table 2
Chemical oxides of off-spec fly ash.

Chemical Composition (% by mass)	
SiO_2	38.19
Al_2O_3	18.76
Fe_2O_3	10.88
SO_3	3.59
CaO	18.8
Na_2O	1.12
MgO	3.6
K_2O	0.98
P_2O_5	0.7
TiO_2	1.31
Total	97.93
LOI	8.47
Unburnt Carbon	7.0
Initial moisture content	1.21

more times to achieve a uniform mixture. After the mixing stage, the mixture was poured into the pelletizer, which was operated at 140 RPM and 45° angle, for 15 min to create spherical pellets. The pellets were cured in an environmental chamber at a temperature of 40 °C and relative humidity (RH) of 30 % for 24 h. The geopolymerization occurred during the curing conditions. In the final stage, the pellets were sintered using a rotary furnace at 1075 °C, 7 RPM, and an angle of 3.50°. The optimized temperature for sintering was obtained using the authors' previously-developed thermodynamics-guided framework.

2.1.2. LWA physical properties

Fig. 1 shows the physical appearance of SPoRA compared with two commercial LWAs, one shale-based LWA (C-LWA) and one slate-based LWA (S-LWA). As can be seen, SPoRA is spherical while C-LWA and S-LWA are angular. The 72 h water absorption and specific gravity in oven dry (OD) and saturated surface dry (SSD) of the SPoRA and commercial LWA were evaluated according to ASTM C 127 and 128 [37,38]. The dry rodded unit weight of the LWA was measured according to ASTM C29. Table 3 shows the physical properties of the fine (particles smaller than 4.75 mm) and coarse (particles greater and equal to 4.75 mm) portions. Particle size distribution for all the LWA passed the ASTM C330 [39] requirement for gradation of structural LWA. As can be seen, SPoRA had the highest 72 h absorption capacity and SSD specific gravity.

2.1.3. Cement

In this study, type I/II ordinary portland cement, based on the ASTM C150 specification [40], was used to prepare concrete samples. The chemical and estimated Bogue compositions of the Portland cement are reported in Table 4.

2.2. Lightweight concrete sample preparation

Three types of concrete samples were prepared with a constant water-to-cement ratio of 0.42 (by mass) using SPoRA, C-LWA, and S-LWA. In order to estimate the uncertainty of the measurements, three replicates were prepared for each concrete sample and each curing period. The mixture proportions for the concrete samples were according to the *ACI* 211.2 procedure as shown in Table 5. The maximum size of aggregate used in this study was 9.5 mm (3/8 in). The aggregates used in the LWC were at the SSD condition. No chemical admixture was added to the concrete mixture. The concrete was mixed with a standard mixer and in accordance with ASTM C305 [41]. After mixing, cylindrical concrete samples were made using 50.8 mm (2 in) by 101.6 mm (4 in) cylindrical molds. The samples were demolded after 24 h and further cured in sealed double plastic bags for 7 days, 14 days, and 28 days at room temperature (23 ± 2 °C).

2.3. Testing methods

Testing methods in this study were divided into testing LWA directly and testing LWC made with LWA. DVSA, XCT, and crushing resistance were performed on the LWA. Measurement of concrete fresh properties, compressive strength, TGA, and isothermal calorimetry was performed on LWC samples to evaluate fresh (before set), mechanical, and hydration properties.

2.3.1. LWA testing methods

2.3.1.1. Dynamic vapor sorption analyzer (DVSA). A DVSA instrument was used to evaluate LWA desorption behavior and characterize LWA pore structure at pore sizes smaller than 50 nm. A fine LWA specimen with an approximate mass of 60 mg was selected for each LWA type. The LWA was soaked in water for 24 h, taken out of the water and a paper towel was used to achieve an SSD condition. Next, the sample was placed in the quartz pan at a constant temperature of 23 ℃ for both the desorption and absorption cycles. The relative humidity (RH) was initially set to 97.5 % and decreased in a single step down to 96 %, then down to 90 % in steps of 2 %, then down to 80 % in steps of 5 %, and finally decreased all the way to 0 % in steps of 10 %. After each step, the RH was kept constant for either 96 h or, if the mass change was less than 0.001 mg over 15 min, then the instrument proceeded to the next step. This same procedure was applied in reverse to raise the RH to 97.5 % for the absorption cycle.

To characterize pores smaller than 50 nm, the Kelvin-Young-Laplace equation [43,44] can be employed to correlate the RH in water-filled pores to pore radius (r) using Equation (1). The reason that only pores smaller than 50 nm can be characterized using the DVSA method is that 97.5 % RH correlates to a pore size of approximately 42 nm. The highest stable RH value that can be achieved using the instrument is 97.5 %. In this equation, γ = water surface tension, RH = relative humidity, V_m= molar mass, R = gas constant i.e., 8.314 J.K^{-1}.mol^{-1}, and T = temperature (K).

$$r = \frac{2\gamma}{\ln(RH)} \times \frac{V_m}{RT} \tag{1}$$

2.3.1.2. X-ray computed tomography (XCT). A Skyscan 1172[1] was used to perform XCT and characterize the LWA pore structure on the same samples that were tested by DVSA. The X-ray tube was set at a voltage of 100 kV and a current of 100 μA, while the voxel size was set at 2.73 μm. An Al + Cu filter was used in the scan. The exposure time per step for a rotation of 180° was ≈ 3.245 s. Two dimensional (2D) projections of the LWA were collected and using the software supplied with the Skyscan 1172, tomographic reconstruction was performed to obtain approximately 1000 2D cross-sectional slices of the LWA. A ring artifact reduction filter was used during tomographic reconstruction to increase the quality of the reconstructed 2D slices. The visualization and calculations presented in this paper were performed using Dragonfly Software [45].

To calculate the porosity and obtain the pore size distribution of the LWA for each dataset, a cubic volume of interest (VOI) with a size of 1092 μm × 1092 μm × 1092 μm was extracted from each LWA. The pore segmentation was done using the Otsu method [46,47]. A plugin of Dragonfly software called OpenPNM[1] [48]was used for the extraction of the pore network of the LWA from the segmented pore-solid phase. The plugin uses an algorithm referred to as SNOW (subnetwork of the over-segmented watershed) [49], which is based on marker-based segmentation for the extraction of pores. This method consists of five steps. In the first step, the distance map of pore space in the binary image is obtained and smoothened using a Gaussian blur filter. In the second step, the peaks are identified in the distance map using a maximum filter with a spherical structuring element of radius R. In the third step, any extraneous peak in the previous step is trimmed, which is the key to avoiding over-segmentation. A detailed description of this method can be found elsewhere [48–50]. In step four, the image is segmented into pore regions using a marker-based watershed segmentation method, where the corrected maxima identified in the previous step are used as the markers. Finally, the segmented image is used to obtain information about the pore and throat (channel) size distributions and the network connectivity.

2.3.1.3. LWA crushing strength. LWA was first sieved into the following size ranges: 4.75 mm to 5.60 mm, 5.60 mm to 6.35 mm, 6.35 mm to 9.5 mm, and 9.5 mm to 12.5 mm. The crushing strength of both bulk and

[1] Certain commercial equipment, software and/or materials are identified in this paper in order to adequately specify the experimental procedure. In no case does such identification imply recommendation or endorsement by the National Institute of Standards and Technology, nor does it imply that the equipment and/or materials used are necessarily the best available for the purpose.

Fig. 1. The physical appearance of SPoRA (left), C-LWA (middle), and S-LWA (right) LWA.

Table 3
Lightweight aggregate physical properties.

Aggregate Type	SPoRA		C-LWA		S-LWA	
Aggregate Size	Fine	Coarse	Fine	Coarse	Fine	Coarse
72 h Absorption (%)	16.4	20.9	15.5	14.7	8.6	10.9
Specific Gravity (OD)	1.56	1.48	1.45	1.27	1.69	1.54
Specific Gravity (SSD)	1.81	1.78	1.68	1.46	1.80	1.60
Dry Rodded Unit Weight (kg/m^3)	978	879	903	762	1040	928

Table 4
Chemical and Bogue composition of OPC Type I/II, with definition of cement chemistry notation in parentheses.

Item	Amount (% by mass)
SiO_2 (S)	18.94
Al_2O_3 (A)	5.00
Fe_2O_3 (F)	4.47
CaO (C)	61.36
MgO	2.96
SO_3	3.55
Na_2O	0.36
K_2O	0.96
C_3S ($3CaO{\cdot}SiO_2$)	57
C_2S ($2CaO{\cdot}SiO_2$)	12
C_3A ($3CaO{\cdot}Al_2O_3$)	5
C_4AF ($4CaO{\cdot}Al_2O_3{\cdot}Fe_2O_3$)	13
Limestone	3.9
Loss on Ignition	2.09

Table 5
Proportions of LWC mixtures obtained using *ACI* 211.2 procedure [42].

Lightweight Concrete	Water (kg/m^3)	Cement (kg/m^3)	Coarse (kg/m^3)	Fine (kg/m^3)
SPoRA	228	544	457	405
C-LWA	228	544	395	372
S-LWA	228	544	483	430

single LWA were measured. The crushing strength of bulk LWA was performed in accordance with European standard specification EN 1097–11 [51]. For the crushing resistance test of LWA, a cylinder with a diameter of 73 mm and a height of 74 mm was used. The LWA sample was poured into the cylinder, and next, the cylinder was placed on a vibration table for 45 s. Additional LWA was added to the cylinder to level the surface. A steel piston with a diameter of 71.25 mm was used to load the LWA in the cylinder. A compressive testing machine was used to apply the loading rate of 0.2 mm/s to the piston. The crushing resistance strength was calculated based on the load ($P_{20\ mm}$) that led to 20 mm displacement for LWA in the cylinder and the cross-sectional area of the cylinder (A), according to Equation (2).

$$\text{Bulk LWA crushing resistance strength} = \frac{P_{20mm}}{\mathrm{A}} \tag{2}$$

To measure the crushing strength of a single LWA, SPoRA with specific size was placed between two parallel plates and were crushed using a compression instrument with 0.98 N force accuracy. The loading speed was set at 2 mm/min. Due to the high variability of the crushing strength of single LWA, 20 samples were tested for each of the four size ranges of the LWA. It has been shown that the crushing strength of spherical ceramics materials with brittle behavior can be calculated using Equation (3) [52,53], where P is the load at failure and D is the distance between the loading points.

$$\text{Single LWA crushing strength} = \frac{2P}{\pi \mathrm{D}^2} \tag{3}$$

2.3.2. LWC testing methods

2.3.2.1. LWC fresh properties. The freshly mixed concrete density, oven-dry density, and equilibrium density of LWC were measured and predicted based on ASTM C567 [54]. The calculated oven-dry density was determined according to Equation (4). In this equation, O_c is the calculated oven-dry density, M_{df} is the mass of dry fine LWA in the batch, M_{dc} is the mass of dry coarse LWA in the batch, M_{cmt} is the mass of cement, 1.2 is a factor to approximate the mass of cement plus chemically combined water, and V is the volume of concrete produced by the batch. In Equation (5), E_c is the calculated equilibrium density.

$$O_c = \frac{M_{df} + M_{dc} + 1.2M_{cmt}}{V} \tag{4}$$

$$E_c = O_c + 50\frac{kg}{m^3} \tag{5}$$

The flow table test was performed to determine the workability of fresh concrete based on ASTM C230 [55]. The flow table consisted of a grip and hinge and a truncated cone that had a height of 50 mm, a base diameter of 100 mm, and a top diameter of 70 mm. The truncated cone was placed in the center of the flow table and filled with the concrete sample in two layers, where 25 S were applied using a spatula in each layer. After smoothing and leveling the concrete surface, the cone was removed. Next, the tests were performed by applying 25 drops from a height of 13 mm in 15 s. The diameter of the spread concrete was measured in six directions. The workability was calculated based on Equation (6).

$$Flow(\%) = \frac{d_{average} - 100mm}{100mm} * 100 \tag{6}$$

where $d_{average}$ is the average value of the measured diameters in six directions (mm), and 100 mm is the base diameter of the cone.

2.3.2.2. Concrete compressive strength. For each concrete sample, three cylindrical samples of 50.8 mm (2 in) diameter and 101.6 mm (4 in) height were tested according to ASTM C 109 [56] to obtain their compressive strength. The average of three values was reported as the compressive strength of each concrete mixture. The compression test was performed at the curing ages of 7 days, 14 days, and 28 days.

2.3.2.3. Thermogravimetric analysis test. Thermogravimetric analysis (TGA) was performed to identify the reactions and subsequent chemical products in LWC. For this purpose, the TA Instrument Q500 IR was used to carry out TGA tests. Nitrogen gas was used as an inert purge gas to detect the sample decomposition due only to temperature changes. The TGA samples were obtained after the compressive strength test from the inner core of the failed samples. It was visually checked to ensure that the broken sample contained all concrete constituents. Broken samples of approximately 200 g were crushed using a mortar and pestle and then sieved through ASTM sieve #200 to achieve powder particles of less than 75 μm in size. A 30 mg concrete powder sample was collected and placed in an alumina crucible pan. The TGA tests were performed by increasing the temperature from the ambient temperature of 23 °C to 900 °C with a 10 °C/*sec* heating rate. The TGA test was performed for the 7 days, 14 days, and 28 days concrete samples.

2.3.2.4. Isothermal calorimetry test. The heat of hydration and degree of hydration in LWC were measured using isothermal calorimetry. Four series of isothermal calorimetry experiments were performed, including three mortar samples containing SPoRA, C-LWA, and S-LWA, and one cement paste. The isothermal calorimetry concrete samples were prepared based on the same mixture proportion values as presented in Table 5, with the exception that coarse LWA was replaced with fine LWA to make mortar samples. The mixture weight prepared for isothermal calorimetry samples was about 10.5 g. It should be noted that fine LWA was used in an SSD condition. The cement and LWA were first placed in a 20 ml ampoule and were gently mixed before introducing water. Water was gently injected into the ampoule using a syringe and then mixed with the solid part for one minute. After the external mixing process, the samples were placed into the isothermal calorimeter cell and isothermal calorimetry carried out at 23 °C ± 0.1. The heat flow was measured for the samples for 12 d. The degree of hydration for the samples was measured according to Equation (7),

$$\alpha_t = \frac{Q_t}{\Delta_{Hydration}} \tag{7}$$

where α_t is the degree of hydration at time t, Q_t is the enthalpy of reactions at time t measured using isothermal calorimetry, and $\Delta_{Hydration}$ is the calculated enthalpy of full hydration. $\Delta_{Hydration}$ was calculated based on the Bogue composition of the cement and the enthalpy of full hydration for C_2S, C_3S, C_3A, and C_4AF, according to Taylor's values [57,58].

3. Results and discussion

3.1. The microstructural appearance of LWA

The 2D slices in Fig. 2 show the microstructure of SPoRA, C-LWA, and S-LWA obtained through XCT. Some similarities could be observed for the pore structure of SPoRA and S-LWA. The pore structure of these LWA was formed by spherical type pores and some large pores were formed by coalescence of smaller pores. The pore structure of C-LWA was notably different than that of SPoRA and S-LWA as it was mainly formed of finer macropores. Balapour et al. [9] showed that the pore structure of LWA is highly dependent on the formation of the liquid phase and its viscosity during sintering. The formation of larger pores in SPoRA and S-LWA could be related to the fact that both LWA had a liquid phase with low viscosity that allowed easier pore expansion and coalescence compared to C-LWA [9,34]. In contrast, C-LWA probably had a high viscosity liquid phase that limited the pore expansion in the LWA and resulted in a finer pore structure.

Fig. 3 shows the solid phase for SPoRA, C-LWA, and S-LWA in three dimensional (3D) obtained through XCT, where the calculated total porosity was 36.5 %, 38.7 %, and 56.8 %, respectively. The calculated porosity for SPoRA, S-LWA, and C-LWA obtained by XCT is smaller than the actual porosity of the LWA due to the limitations of the XCT resolution [59]. Pores smaller than 2.73 μm, which can contribute to the total porosity, are not captured through XCT (see Fig. 5 and discussion in Section 3.3). The closed porosity for the SPoRA, C-LWA, and S-LWA were 3.2 %, 0.17 %, and 3.8 %, respectively, indicating that the pore structure type (large spherical pores) of SPoRA and S-LWA can lead to somewhat higher closed porosity.

3.2. LWA water desorption behavior

Fig. 4 shows the water desorption isotherms for SPoRA, C-LWA, and S-LWA obtained through DVSA. The desorption behavior of LWA is crucial for concrete internal curing applications. The desorption isotherms demonstrate how the LWA releases water to the cement paste

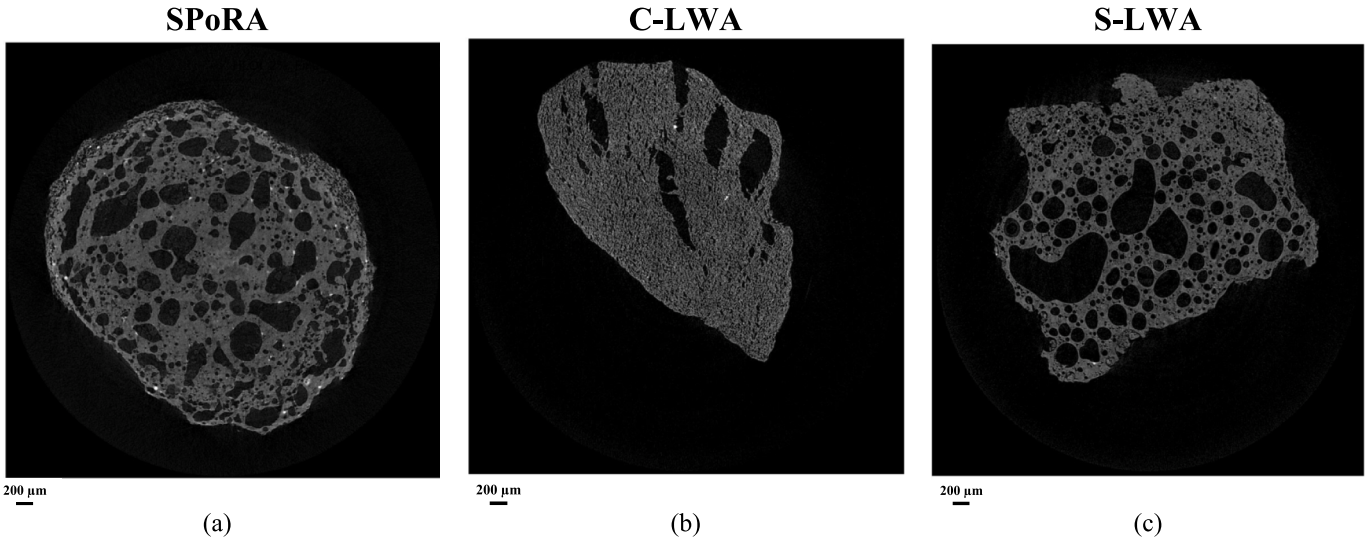

Fig. 2. 2D slices from XCT of (a) SPoRA, (b) C-LWA, and (c) S-LWA LWA; each 2D slice represents the middle cross-section of the LWA.

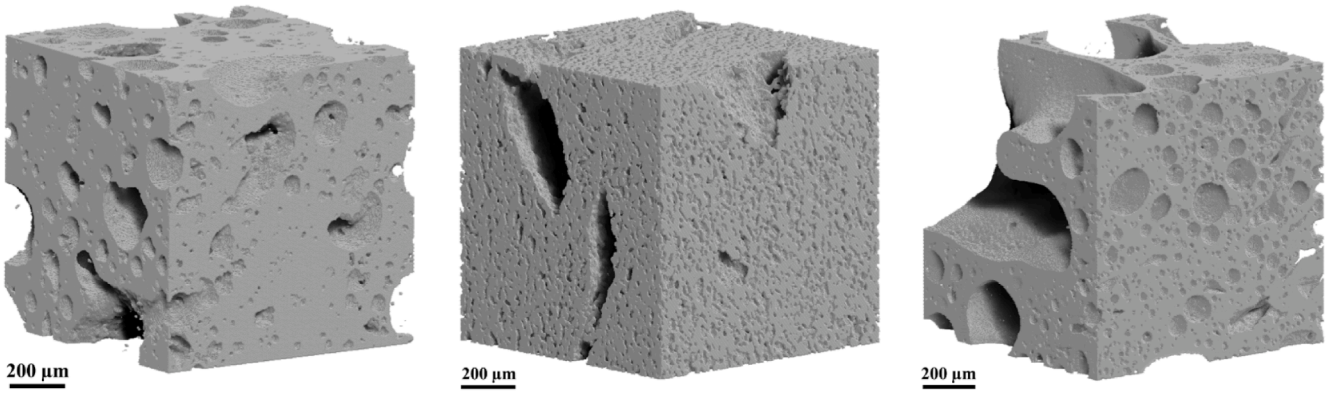

Fig. 3. 3D solid phase, total porosity (φ) and closed porosity obtained by XCT for (a) SPoRA, (b) C-LWA, and (c) S-LWA LWA.

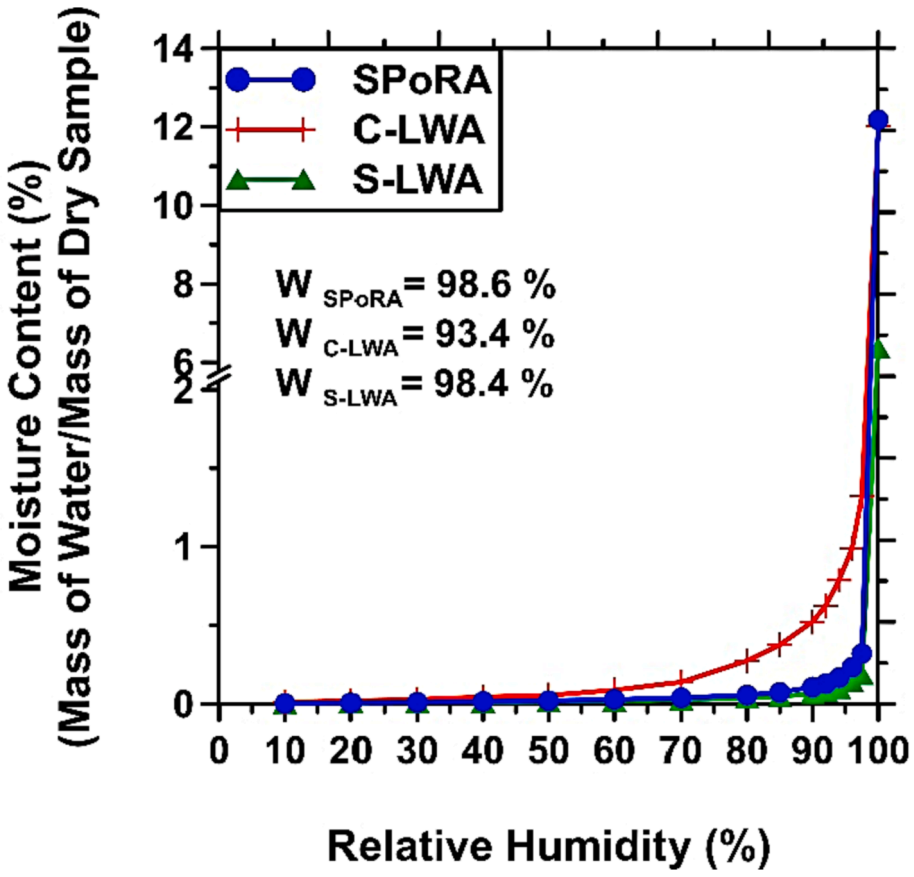

Fig. 4. The desorption isotherms for SPoRA, C-LWA, and S-LWA: Note that the y-axis (Moisture Content (%)) is broken at 2 for a better representation of the complete range of moisture content data.

matrix during the self-desiccation period [8]. As can be seen, SPoRA and S-LWA had a sudden release of water as the RH dropped to 97.5 %. C-LWA also released a considerable portion of its absorbed water as RH dropped to 97.5 %; however, it can be seen there was a gradual water release as the RH further decreased. This behavior indicates that SPoRA and S-LWA had coarser pore structures than C-LWA, and due to lower capillary suction force, they were able to release the absorbed water at a higher RH. According to ASTM C1761 [60], the LWA has to release more than 85 % of its absorbed water as RH drops to 94 % RH. SPoRA, C-LWA, and S-LWA released 98.6 %, 93.4 %, and 98.4 % of their absorbed water at 94 % RH, respectively, showing that all comply with the ASTM C1761 requirement. Therefore, they all have a potential for use in concrete internal curing. As can be seen, SPoRA and C-LWA had a water absorption value of 12 % at 100 % RH (i.e., SSD). In contrast, the water absorption for S-LWA was about 6 % at 100 % RH. Although S-LWA showed good desorption behavior, its low absorption capacity means that it can supply less water than SPoRA and C-LWA during concrete internal curing.

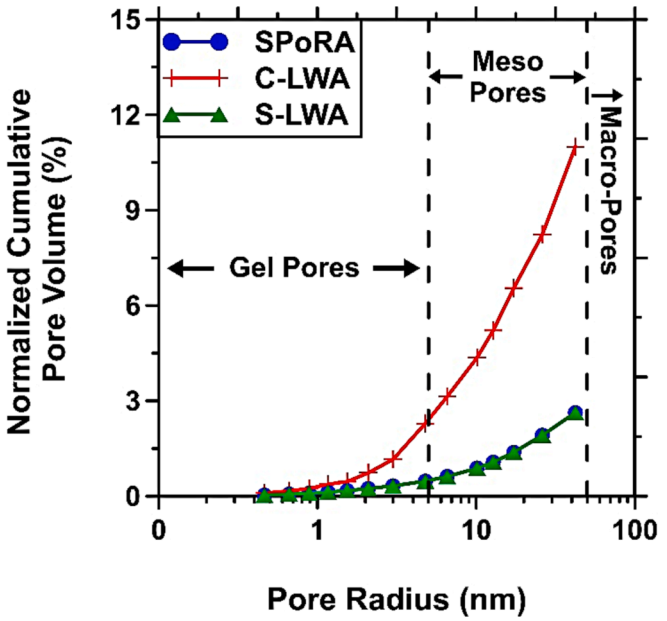

Fig. 5. The pore size distribution for SPoRA, C-LWA, and S-LWA at pore sizes smaller than 50 nm obtained through DVSA.

3.3. LWA pore size distribution

Fig. 5 shows the pore size distribution of SPoRA, C-LWA, and S-LWA for the pores smaller than 50 nm obtained through DVSA. Pores were categorized as gelpores (smaller than 5 nm), mesopores (between 5 nm and 50 nm), and macropores (greater than 50 nm). As can be seen, SPoRA and S-LWA had a similar pore structure in this size range, and only about 3 % of the pores were classified as gel and mesopores, while more than 97 % of the pores were classified as macropores. In contrast, C-LWA had a finer pore structure, with about 11 % of pores classified as gel and mesopores, and about 89 % of the pores classified as macropores. As was previously mentioned, one of the most important parameters that can control LWA pore formation is the viscosity of the liquid phase formed during sintering. As was observed from the XCT 2D slices, it can be inferred that SPoRA and S-LWA had a low viscosity liquid phase that facilitated the expansion of gas-filled pores in the liquid phase during sintering and consequently a minimal amount (less than 3 %) of pores smaller than 50 nm were formed. In contrast, the apparent high viscosity of the liquid phase in the C-LWA limited the expansion of gas-filled pores and led to the formation of a higher number of gelpores and mesopores.

Fig. 6 shows the cumulative normalized porosity share of different pore categories in LWA obtained using XCT. D_{50} shown on the figure is defined as the pore size at which the cumulative normalized porosity reaches 50 % of the total porosity. The value of D_{50} for SPoRA, C-LWA, and S-LWA was 140 μm, 71 μm, and 264 μm, respectively. This observation indicates that for C-LWA, 50 % of the porosity was comprised of pores smaller than 71 μm, which clearly demonstrated that C-LWA had a finer pore structure compared to SPoRA and S-LWA. SPoRA LWA had an intermediate pore structure compared to other two LWAs, where 50 % of the porosity was contributed by pores smaller than 140 μm. Finally, S-LWA clearly had the coarsest pore structure among the LWAs since it had the largest value of D_{50}.

3.4. LWA crushing strength

The crushing resistance of LWA plays a major role in terms of the overall strength of concrete and may govern the failure modes of the mechanical testing [61]. Furthermore, LWA crushing resistance has a significant impact on the concrete modulus of elasticity [62]. Fig. 7 shows the crushing strength of bulk LWA in different size categories. SPoRA had the lowest crushing strength in comparison to C-LWA and S-LWA in all size categories. Moreover, as SPoRA size increased, the crushing strength decreased. For C-LWA, as the LWA size range increased from [4.75 mm to 5.6 mm] to [6.35 mm to 9.5 mm], the crushing strength decreased similar to behavior of SPoRA. However, the crushing strength stayed constant as the LWA size further increased. In contrast to SPoRA and C-LWA, the crushing strength of S-LWA increased as the LWA size range increased from [4.75 mm to 5.60 mm] to [6.35 mm to 9.50 mm]. The average crushing strength of the S-LWA was constant as its size range further increased.

A possible reason for the lower crushing strength of SPoRA compared to C-LWA and S-LWA could be related to the respective manufacturing

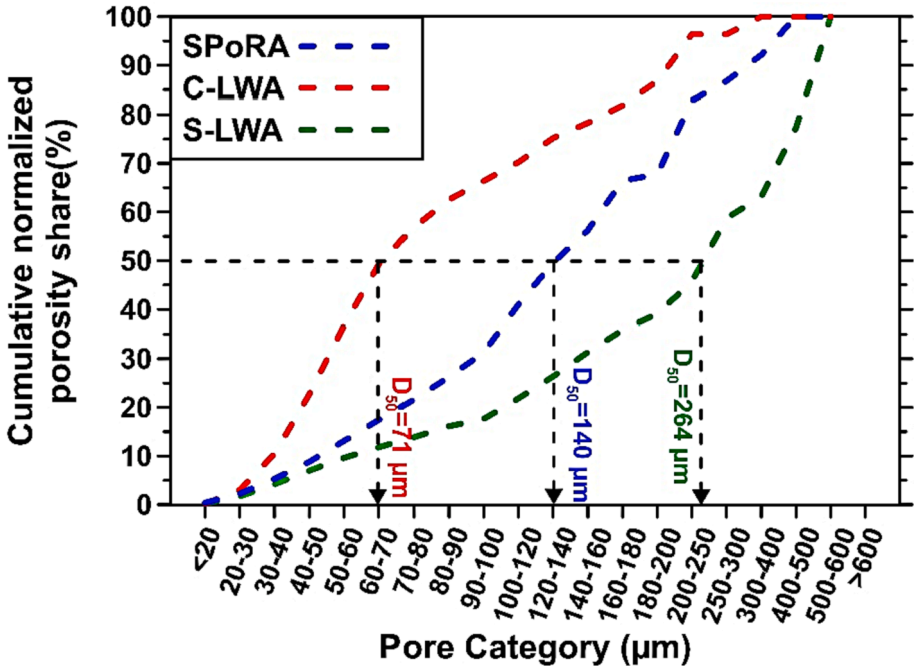

Fig. 6. Normalized porosity share of pores greater than 2.73 μm for SPoRA, C-LWA, and S-LWA obtained through XCT.

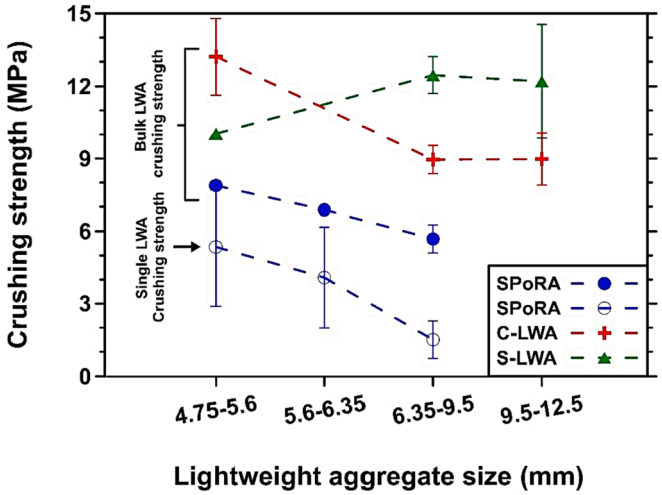

Fig. 7. Bulk crushing strength of SPoRA, C-LWA, and S-LWA in different sizes; the hollow circle symbols show the crushing strength of SPoRA single-particle (the bars for bulk LWA and single LWA show ± one standard deviation for three and twenty replicates, respectively).

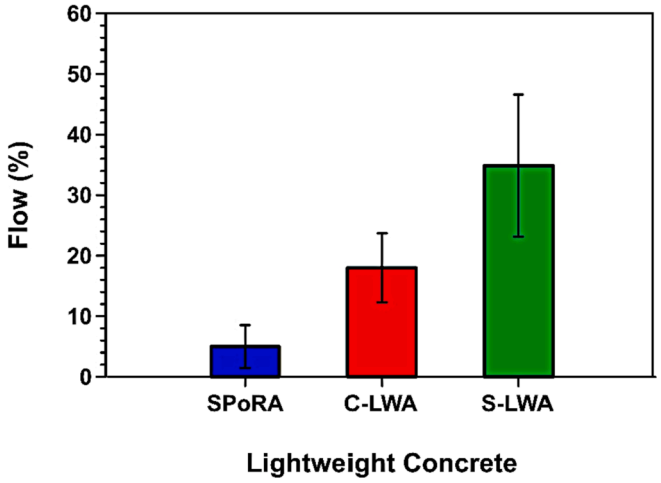

Fig. 8. The flow percentage for lightweight concrete prepared with SPoRA, C-LWA, and S-LWA.

processes. For the commercial LWA, big lumps of shale or slate are sintered in a rotary furnace for a prolonged time and then are crushed to the appropriate size. This type of sintering might help with the increase in the strength of the LWA. For SPoRA, fresh aggregate is made using a pelletizer to form the appropriate particle size, and then are sintered only for a few minutes in a rotary furnace.

Based on the pore size distribution of LWA, one might expect a lower crushing strength for S-LWA due to its coarser pore structure (see Fig. 3 and Fig. 6) and macropores that were larger compared to the other LWA. However, it should be noted that the crushing strength of a porous material depends not only on the porosity and pore structure of the LWA, but also on the solid phase and the pore distribution within the solid phase [63]. The strength of the solid phase can be influenced by mineralogical composition, the amount of liquid phase, and the density of microcracks caused by thermal shock during sintering [63].

The hollow circles in Fig. 7 show the crushing strength of single SPoRA particles. The SPoRA single-particle crushing strength followed the same trend as the bulk LWA crushing strength. This observation further confirmed that for SPoRA the strength decreased as the particle diameter increased. This could be related to the inherent properties of brittle materials; with increasing sample volume the probability of a critical flaw that leads to failure for a given stress increases [64,65].

3.5. Lightweight concrete workability and fresh density

LWC pumpability, which is particularly important for ready-mix concrete producers [11], is directly related to workability (rheology). LWA used in the production of LWC usually has high water absorption, and if this absorption capacity is not accounted for, the workability can be altered. For instance, the use of unsaturated LWA can decrease the workability of concrete significantly due to absorption of available mixture water by LWA and consequently reducing the water to cement mass ratio (w/c). Therefore, to control LWC workability, the LWA is usually presoaked in water for 24 h to 72 h and only then is used for LWC production. To further increase the workability of fresh LWC (and therefore increase pumpability), the use of spherical LWA can be considered [66]. In this study, SPoRA was spherical, while C-LWA and S-LWA were angular. Fig. 8 shows the results of the flow table test for measuring the workability of the fresh LWC. It was anticipated that the spherical shape of SPoRA could increase workability compared to LWC prepared with angular LWA. However, the flow percentage for SPoRA LWC was 5 % and that of C-LWA and S-LWA LWC were 18 % and 34.9 %, respectively. Further investigation is required to understand if the obtained flow percentage of SPoRA causes technical challenges for concrete pouring at larger scales. A potential reason for lower flow percentage of SPoRA LWC could be related to insufficient water saturation of the SPoRA before concrete preparation, which resulted in absorbing the mixture water during mixing stage and reducing the flow percentage. Another possible reason for the reduction of flow percentage for SPoRA LWC could be related to the use of NaOH as the fluxing agent for the production of the SPoRA, where a reaction between SPoRA and cement resulted in the observed reduction. As such, the pH of a mixture of water and LWA was measured over time.

Fig. 9 shows the pH of a mixture of water and LWA with a 1:1 mass ratio over time. As can be seen, all the LWA had a pH of greater than 7, whereas a much higher pH was measured for SPoRA right after mixing. Approximately an hour after mixing the LWA with water, the pH level slightly increased for all the LWA and stayed constant after that. SPoRA had higher alkalinity compared to C-LWA and S-LWA, due to the use of NaOH as the fluxing agent for sintering. It is postulated that some of the added NaOH is capsulated in the liquid phase during sintering. However, the portion that was not capsulated was probably washed into the water and increased the pH value. Further research is required to test this hypothesis and evaluate the effect of using NaOH as fluxing agent on increasing the pH of the concrete mixing water.

Since the LWA is added to the concrete mixture in the SSD condition, the fresh density of LWC is directly affected by the LWA specific gravity. From Table 3, SPoRA had the highest SSD specific gravity, followed by S-LWA; C-LWA had the lowest value. Fig. 10 shows the measured fresh density of SPoRA, C-LWA, and S-LWA LWC, which follows the same trend.

3.6. Lightweight concrete density and compressive strength

Fig. 11 shows the calculated equilibrium density (ASTM C330) and the measured density of LWC samples at 7 days, 14 days, and 28 days. All the LWC had a calculated equilibrium density of less than 1680 kg/m^3, which was the target value for this study based on the ASTM C330 specification. SPoRA LWC had the highest density compared to C-LWA and S-LWA LWC at all three ages. The difference between measured densities and equilibrium density is related to the moisture that is retained in the LWC samples, which was not given a chance to be released as the samples were cured in a sealed condition (moisture transfer between sample and environment prevented).

Fig. 12 shows the compressive strength of three LWCs at 7 days, 14 days, and 28 days. For SPoRA LWC and C-LWA LWC, the average compressive strengths at 14 days were slightly less than the 7 days

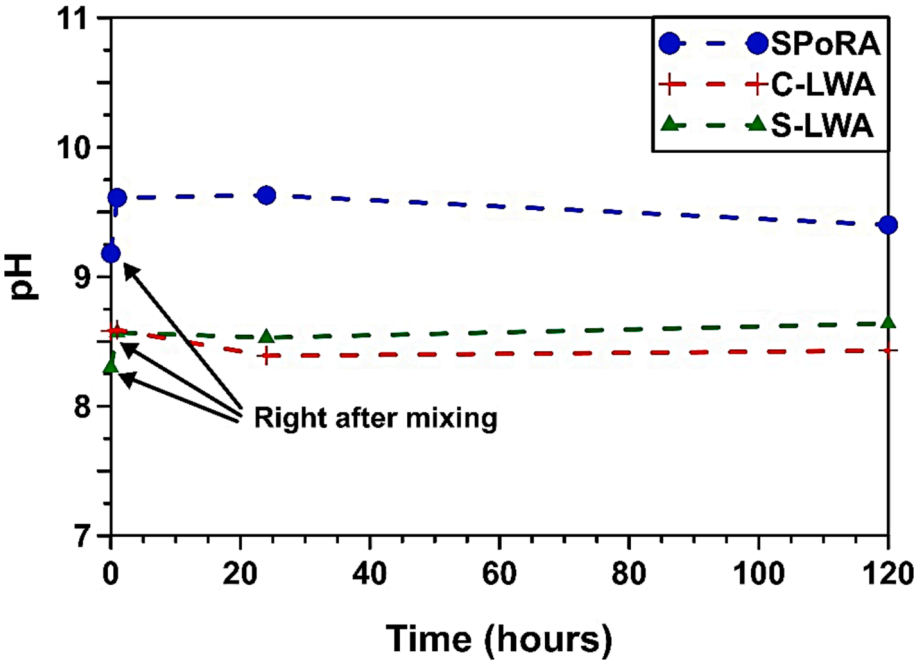

Fig. 9. pH of the SPoRA and water mixture over time.

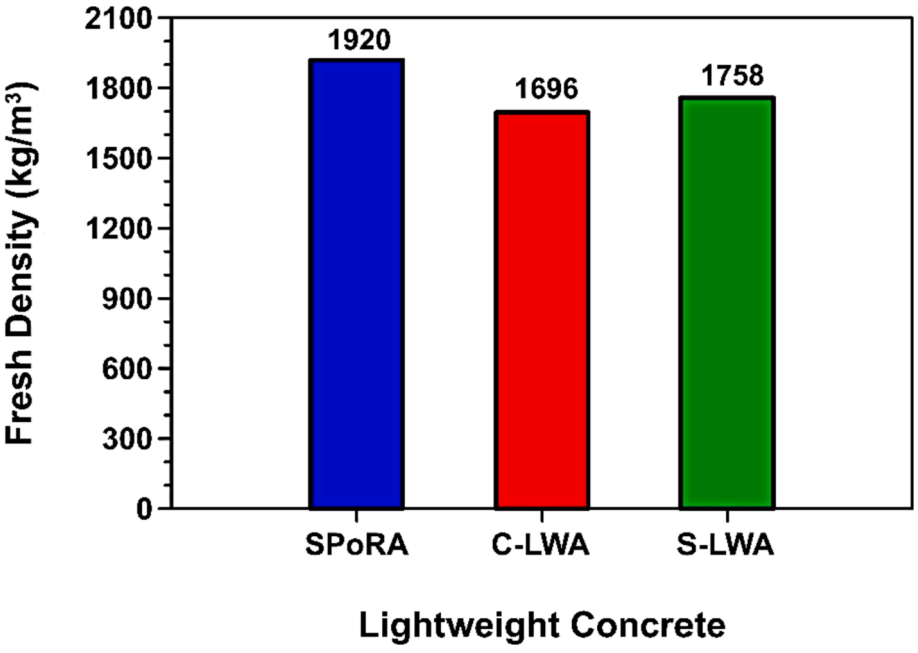

Fig. 10. Fresh density of lightweight concrete prepared with SPoRA, C-LWA, and S-LWA.

values. The 7 days and 14 days values for SPoRA LWC were within the range of standard deviation. For C-LWA LWC, this decrease was more than the standard deviations; the reason behind this reduction is not clear and needs further investigation. In contrast, for S-LWA LWC the compressive strength increased at 14 days compared to 7 days. The 28 days compressive strength of all LWCs was higher than that of their 7 d and 14 days values. This observation indicated that continuous cement hydration through the provided internal curing water resulted in higher compressive strength.

According to ASTM C330, structural LWC with a maximum calculated equilibrium density of 1680 kg/m^3 must have a minimum compressive strength of 21 MPa at 28 days. As can be seen, all three LWC mixtures passed this requirement. Another important observation is that the LWC compressive strength was not correlated to the bulk LWA crushing strength (see Fig. 7). Even though SPoRA had the lowest crushing strength among the three LWAs, it had a 28 days compressive strength of about 30 MPa, almost equal to that of S-LWA LWC. This observation indicates that the LWA crushing strength does not have a significant impact on the final compressive strength of the LWC composite.

3.7. Thermogravimetric analysis

Fig. 13 shows the differential TGA curves for LWC powder samples at

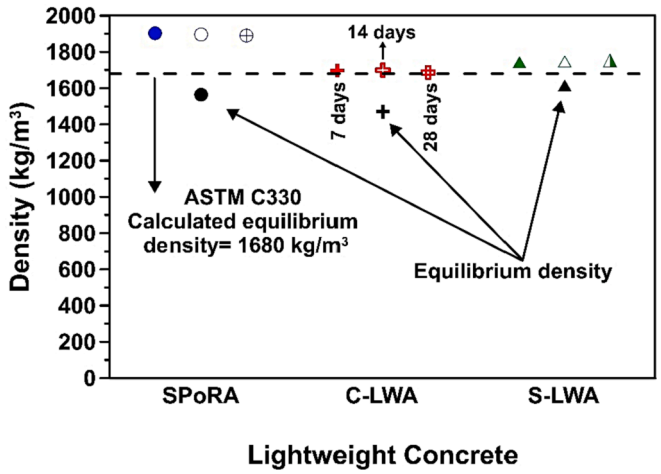

Fig. 11. Lightweight concrete density at 7 days, 14 days, and 28 days; the black symbols show the calculated equilibrium density.

7 days, 14 days, and 28 days. Each peak in the differential TGA curve is related to the decomposition of a phase over a specific temperature change, which is identified on the figure. C-LWA and S-LWA LWC had similar thermal behavior at different ages. The differential TGA curves for SPoRA LWC showed the formation of a smaller amount of $Ca(OH)_2$, which is the byproduct of cement hydration. Two potential reasons could be considered for this observation: (i) pozzolanic reaction between the SPoRA and cement paste resulted in $Ca(OH)_2$ reduction or (ii) the interference of NaOH as the fluxing agent with cement reactions suppressed the hydration of cement and reduced the $Ca(OH)_2$ in SPoRA LWC. Future investigation is required to more fully understand the possible interactions between SPoRA and cement during hydration.

The peaks in the range of 600 °C to 700 °C could be related to carbonate phases formed in the concrete, where the peaks were larger for 7 days SPoRA LWC. This could be related to the fact that the fly ash used for the production of SPoRA had a high free carbon content, which potentially led to the formation of higher content of carbonate phases through the reaction of fine SPoRA. However, as the samples aged, the carbonate-type phases had a similar decomposition intensity in the LWC. A strong phase decomposition was observed for SPoRA LWC starting at 750 ℃, which could be related to the decomposition of phases available in the SPoRA. The peak intensity did not change notably over time. As such, it might be inferred that the SPoRA possessed an inert phase that potentially did not interfere with the cement hydration. However, further investigation is required to determine the exact nature of this phase and its reactivity with cementitious phases.

3.8. Isothermal calorimetry

Fig. 14 (a) shows the normalized heat of hydration for cement paste and SPoRA, C-LWA, and S-LWA mortars over 12 days period. As can be seen, the control cement paste (no LWA) had the lowest heat release during the hydration compared to the mortar samples. The higher heat of hydration for the mortar samples was related to the extra water that the LWA provided through the internal curing mechanism, leading to a higher amount of cement hydration. This observation indicated that all three LWAs were successful in releasing water to the cement to promote hydration. Among the mortar samples, C-LWA and S-LWA mortars had the highest heat of hydration and demonstrated a very similar behavior for the heat of hydration. In contrast, the SPoRA mortar sample had a slightly lower hydration heat than C-LWA and S-LWA mortars. This observation contrasted with what was expected for SPoRA. As indicated in Table 3, SPoRA had the highest water absorption capacity among the LWA. As such, it was expected that SPoRA could release more water to the cement paste and result in a higher heat of hydration. A possible reduction for the heat of hydration in the SPoRA mortar sample could be related to the chemical composition of SPoRA. As was observed in Fig. 9, SPoRA had higher alkalinity compared to other LWA. It is expected that the excess NaOH used as the fluxing agent could influence the hydration of cement in the matrix [67]. Mota et al. [68] also observed that the addition of NaOH to cement could decrease the degree of cement hydration at later ages; however, they stated that the reason for this reduction was unclear. Fig. 14 (b) shows the measured degree of hydration for cement paste and for the SPoRA, C-LWA, and S-LWA mortar samples, which follows the same trend as that of the heat of hydration. The 12 days degree of hydration for cement paste, and the SPoRA, C-

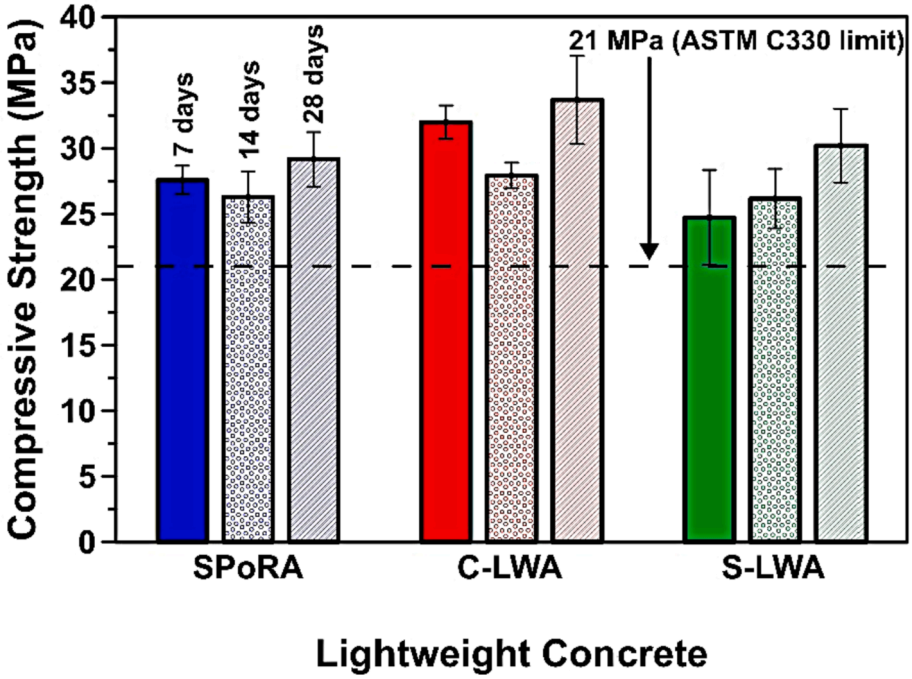

Fig. 12. (a) Compressive strength of lightweight concrete prepared with SPoRA, C-LWA, and S-LWA at 7 days, 14 days, and 28 days.

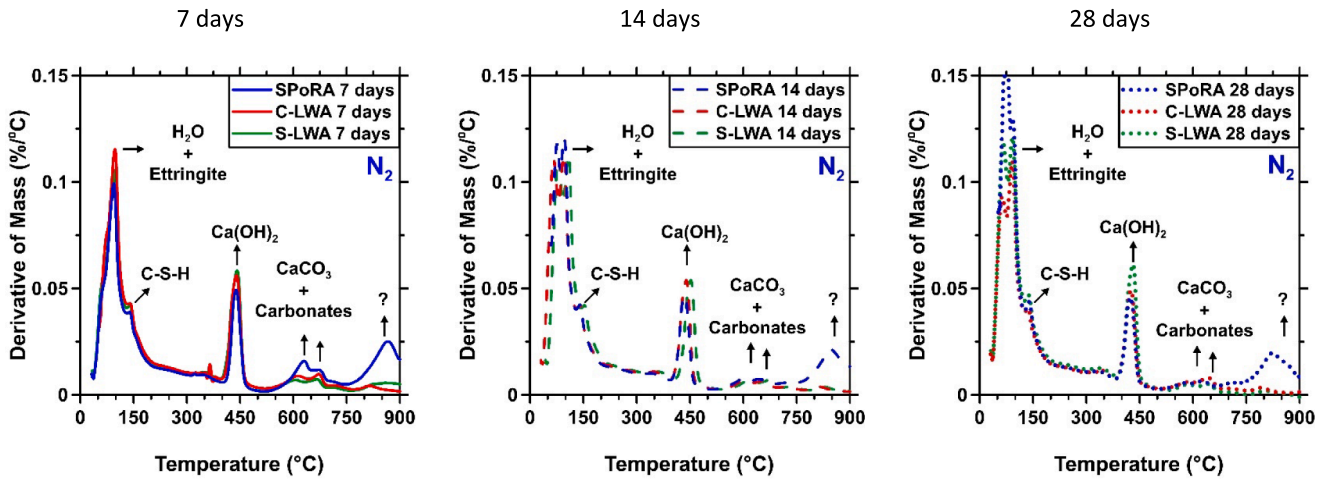

Fig. 13. The differential thermogravimetric analysis curves for concrete samples prepared with SPoRA, C-LWA, and S-LWA at 7 days, 14 days, and 28 days.

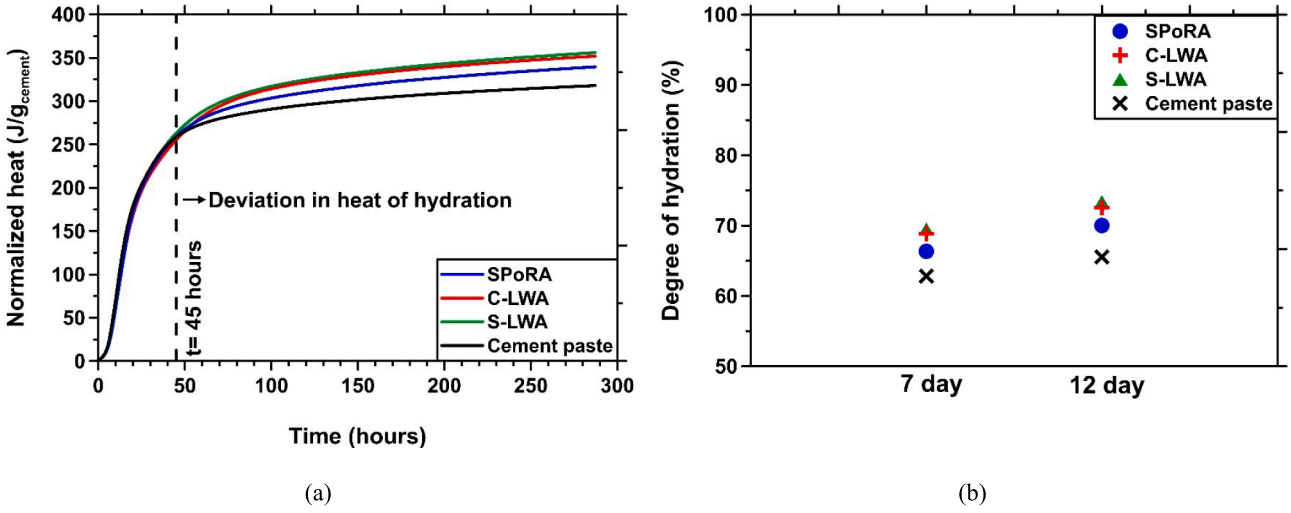

Fig. 14. (a) Normalized heat of hydration for cement and mortar samples over a period of 12 days and (b) their associated degree of hydration.

LWA, and S-LWA mortar samples, was 65.6 %, 70 %, 72.6 %, and 73.4 %, respectively. It should be noted that as the heat of hydration during the first 45 min was not measured, the actual degree of hydration for the samples could be slightly higher. Future research is required to fully understand the hydration properties of SPoRA mortar samples at early age (first 45 min) and at later ages.

4. Summary and conclusions

This study evaluated and compared the physical and engineering properties of fly ash-based LWA (i.e., SPoRA) and its associated LWC with two commercial LWAs. The SPoRA was designed based on a thermodynamics-guided framework [69] through a lab pilot-scale manufacturing process. Physical properties (i.e., specific gravity, water absorption, and dry rodded unit weight, and crushing resistance) and pore structure of the fly ash-based LWA were characterized and compared with shale (C-LWA) and slate (S-LWA) based commercial LWA available in the US market. Fresh, mechanical, and hydration properties of LWC were characterized. The following conclusions can be drawn based on this study:

The desorption isotherms indicated that SPoRA along with the other LWAs complied with the ASTM C1761 requirement for concrete internal curing applications, i.e., releasing more than 85 % of absorbed water as the RH falls below 94 %. However, superior 72 h absorption capacity of fine and coarse SPoRA compared to commercial LWA suggested that SPoRA can provide higher internal curing capacity to avert the shrinkage of concrete during self-desiccation.

The pore size distribution of the LWA obtained through DVSA and the Kelvin-Young-Laplace equation indicated that for SPoRA and S-LWA more than 97 % of the pores were classified as macropores (i.e., pores larger than 50 nm). In contrast, for C-LWA, 89 % of the pores were classified as macropores. This observation alongside X-CT further confirmed the coarser pore structure of SPoRA, which was related to the lower viscosity of the liquid phase formed in the LWA during sintering, which facilitated gas-filled pore expansion in the LWA. Characterization of pores greater than 2.73 μm using XCT indicated an intermediate macropore structure for SPoRA, where it had a D_{50} larger than C-LWA and smaller than S-LWA. This intermediate pore structure provided greater water absorption capacity and water desorption performance compared to S-LWA and C-LWA.

SPoRA had an average crushing strength of 6.8 MPa which was lower than that of commercial LWA. Two reasons for this observation could be (i) different manufacturing processes and (ii) different LWA solid matrix properties. The SPoRA production process entailed only a few minutes of sintering while that of C-LWA and S-LWA included sintering for a prolonged time (close to one hour). However, SPoRA and S-LWA LWC

mixtures had almost the same 28 days compressive strength (about 30 MPa), suggesting that the LWA crushing strength is probably not the most crucial factor that controls the strength of the LWC composite.

It was expected that using SPoRA for LWC preparation would increase the workability of fresh LWC due to its spherical shape. However, it was observed that SPoRA reduced the workability of LWC compared to LWC prepared with C-LWA and S-LWA. Two potential reasons behind this observation were (i) insufficient water saturation of SPoRA that resulted in absorption of the mixture water during mixing, and (ii) use of NaOH as the fluxing agent for SPoRA LWA which resulted in higher alkalinity for SPoRA compared to other LWA.

DTGA curves indicated a lower $Ca(OH)_2$ decomposition intensity for SPoRA LWC compared to C-LWA and S-LWA LWC, which could be related to (i) a lower degree of hydration for SPoRA LWC or (ii) SPoRA pozzolanic reactivity. Isothermal calorimetry indicated that all the mortar samples were successful in increasing the heat of hydration compared to that of cement paste by providing internal curing water. However, the SPoRA mortar samples demonstrated a slightly lower heat of hydration compared to the C-LWA and S-LWA mortar samples, even though SPoRA, due to its higher water absorption capacity, could provide more internal curing water and further increase the heat of hydration. The reason behind this reduction in the heat of hydration may be related to the use of NaOH as the fluxing agent in SPoRA production, which might interfere with cement hydration.

This study shows that manufacturing of waste fly ash-based LWA (SPoRA) can be successfully scaled-up using a pelletizer and rotary furnace at the lab-scale. It is envisioned that this manufacturing can be further scaled-up for production of SPoRA at the industrial scale. It was shown SPoRA manufactured at lab pilot-scale meets the ASTM C330 standard requirements for structural LWA and could be a competitive alternative for C-LWA and S-LWA. In addition, it was shown that the LWC incorporating SPoRA meets the ASTM C330 requirements for structural LWC.

Future studies involve investigating the effect of the fluxing agent used (e.g., NaOH) for LWA production on the interaction of cement and the LWA. In addition, the applicability of using an alternative fluxing agent will be investigated. It is believed such investigation provides a better understanding of the observed reduction in the workability of SPoRA LWC compared to commercial LWAs. Furthermore, the effect of SPoRA on microstructural and durability properties of concrete will be studied to ensure the suitability of this LWA for concrete applications. Since SPoRA is produced from waste fly ash, leachability of various constituents from the waste fly ash is of potential concern and so is another aim of future research to ensure safe use of these materials in concrete applications.

CRediT authorship contribution statement

Mohammad Balapour: Conceptualization, Formal analysis, Investigation, Visualization, Writing – original draft, Writing – review & editing, Funding acquisition, Methodology. **Mohammad H. Khaneghahi:** Investigation, Writing – review & editing. **Edward J. Garboczi:** Investigation, Writing – review & editing. **Yick G. Hsuan:** Writing – review & editing. **Diana E. Hun:** Supervision, Writing – review & editing. **Yaghoob Farnam:** Supervision, Writing – review & editing, Funding acquisition, Project administration.

Declaration of Competing Interest

The authors declare that they have no known competing financial interests or personal relationships that could have appeared to influence the work reported in this paper.

Acknowledgments

This work was supported in part by the National Science Foundation (NSF) under PFI– TT 1918838 grant and was performed at Drexel University in the Advanced and Sustainable Infrastructure Materials (ASIM) Lab. Dr. Balapour is thankful to NSF for the NSF-INTERN award that made this study possible. Any opinions, findings, and conclusions, or recommendations expressed in this material are those of the authors and do not necessarily reflect the views of the NSF.

References

[1] S. Chandra, L. Berntsson, Lightweight Aggregate Concrete, Elsevier, 2002.
[2] D. Sari, A.G. Pasamehmetoglu, The effects of gradation and admixture on the pumice lightweight aggregate concrete, Cem. Concr. Res. 35 (5) (2005) 936–942.
[3] A. Kılıç, C.D. Atiş, E. Yaşar, F. Özcan, High-strength lightweight concrete made with scoria aggregate containing mineral admixtures, Cem. Concr. Res. 33 (10) (2003) 1595–1599.
[4] M. Franus, D. Barnat-Hunek, M. Wdowin, Utilization of sewage sludge in the manufacture of lightweight aggregate, Environ. Monit. Assess. 188 (2016) 10.
[5] J. Castro, L. Keiser, M. Golias, J. Weiss, Absorption and desorption properties of fine lightweight aggregate for application to internally cured concrete mixtures, Cem. Concr. Compos. 33 (2011) 1001–1008, https://doi.org/10.1016/j.cemconcomp.2011.07.006.
[6] M. Zhao, M. Zhao, M. Chen, J. Li, D. Law, An experimental study on strength and toughness of steel fiber reinforced expanded-shale lightweight concrete, Constr. Build. Mater. 183 (2018) 493–501.
[7] C. Arriagada, I. Navarrete, M. Lopez, Understanding the effect of porosity on the mechanical and thermal performance of glass foam lightweight aggregates and the influence of production factors, Constr. Build. Mater. 228 (2019), 116746.
[8] M. Balapour, W. Zhao, E.J. Garboczi, N.Y. Oo, S. Spatari, Y.G. Hsuan, P. Billen, Y. Farnam, Potential use of lightweight aggregate (LWA) produced from bottom coal ash for internal curing of concrete systems, Cem. Concr. Compos. 105 (2020), 103428.
[9] M. Balapour, R. Rao, E.J. Garboczi, S. Spatari, Y.G. Hsuan, P. Billen, Y. Farnam, Thermochemical principles of the production of lightweight aggregates from waste coal bottom ash, J. Am. Ceram. Soc. 104 (1) (2021) 613–634.
[10] M. Balapour, R. Rao, S. Spatari, Y.G. Hsuan, Y. Farnam, Engineering Properties of Fly Ash-Based Lightweight Aggregate, in: World Coal Ash Conf. (WOCA), St. Louis, MO, May 13-16, 2019.
[11] A. Mousa, M. Mahgoub, M. Hussein, Lightweight concrete in America: presence and challenges, Sustain. Prod. Consum. 15 (2018) 131–144.
[12] M. Dondi, P. Cappelletti, M. D'Amore, R. de Gennaro, S.F. Graziano, A. Langella, M. Raimondo, C. Zanelli, Lightweight aggregates from waste materials: Reappraisal of expansion behavior and prediction schemes for bloating, Constr. Build. Mater. 127 (2016) 394–409, https://doi.org/10.1016/j.conbuildmat.2016.09.111.
[13] A.A. Ramezanianpour, Cement replacement materials, Springer Geochemistry/Mineralogy 10 (2014) 973–978.
[14] ASTM C618-19, Standard Specification for Coal Fly Ash and Raw or Calcined Natural Pozzolan for use in Concrete, West Conshohocken, PA, USA ASTM Int. (2019).
[15] M. AASHTO, 295-19: Standard Specification for Coal Fly Ash and Raw or Calcined Natural Pozzolan for Use in Concrete, (2019).
[16] American Coal Ash Association, ACCA 2019 CCP Survey Results, (2019).
[17] M.A. Hitt, Coal Ash and Clean Water: The Dan River Spill Five Years Later, (2019). https://www.sierraclub.org/articles/2019/02/coal-ash-and-clean-water-dan-river-spill-five-years-later.
[18] A.J. Bednar, D.E. Averett, J.M. Seiter, B. Lafferty, W.T. Jones, C.A. Hayes, M. A. Chappell, J.U. Clarke, J.A. Steevens, Characterization of metals released from coal fly ash during dredging at the Kingston ash recovery project, Chemosphere. 92 (11) (2013) 1563–1570.
[19] M.S. Nadesan, P. Dinakar, Structural concrete using sintered flyash lightweight aggregate: A review, Constr. Build. Mater. 154 (2017) 928–944.
[20] S. Sahoo, A.K. Selvaraju, Mechanical characterization of structural lightweight aggregate concrete made with sintered fly ash aggregates and synthetic fibres, Cem. Concr. Compos. 113 (2020), 103712.
[21] Y.-L. Wei, S.-H. Cheng, W.-J. Chen, Y.-H. Lu, K. Chen, P.-C. Wu, Influence of various sodium salt species on formation mechanism of lightweight aggregates made from coal fly ash-based material, Constr. Build. Mater. 239 (2020), 117890.
[22] M. Balapour, Conversion of Waste Coal Combustion Ash to Value-Added Construction Lightweight Aggregates Through a Holistic Thermodynamics-Guided Manufacturing Framework, Drexel University, 2021.
[23] K. Ramamurthy, K.I. Harikrishnan, Influence of binders on properties of sintered fly ash aggregate, Cem. Concr. Compos. 28 (1) (2006) 33–38.
[24] A. Terzić, L. Pezo, V. Mitić, Z. Radojević, Artificial fly ash based aggregates properties influence on lightweight concrete performances, Ceram. Int. 41 (2) (2015) 2714–2726.
[25] A. Sarabèr, R. Overhof, T. Green, J. Pels, Artificial lightweight aggregates as utilization for future ashes–A case study, Waste Manag. 32 (1) (2012) 144–152.
[26] M. Zahedi, K. Jafari, F. Rajabipour, Properties and durability of concrete containing fluidized bed combustion (FBC) fly ash, Constr. Build. Mater. 258 (2020), 119663.
[27] I. Diaz-Loya, M. Juenger, S. Seraj, R. Minkara, Extending supplementary cementitious material resources: Reclaimed and remediated fly ash and natural pozzolans, Cem. Concr. Compos. 101 (2019) 44–51.

[28] T.Y. Lo, H. Cui, S.A. Memon, T. Noguchi, Manufacturing of sintered lightweight aggregate using high-carbon fly ash and its effect on the mechanical properties and microstructure of concrete, J. Clean. Prod. 112 (2016) 753–762.
[29] W.H. Chesner, R.J. Collins, M.H. MacKay, J. Emery, User guidelines for waste and by-product materials in pavement construction, Recycled Mater. Resour. Center (2002).
[30] M. Balapour, T. Thway, R. Rao, N. Moser, E.J. Garboczi, Y.G. Hsuan, Y. Farnam, A thermodynamics-guided framework to design lightweight aggregate from waste coal combustion fly ash, Resour. Conserv. Recycl. 178 (2022), 106050.
[31] C.M. Riley, Relation of chemical properties to the bloating of clays, J. Am. Ceram. Soc. 34 (4) (1951) 121–128.
[32] J.C. van Dyk, F.B. Waanders, S.A. Benson, M.L. Laumb, K. Hack, Viscosity predictions of the slag composition of gasified coal, utilizing FactSage equilibrium modelling, Fuel. 88 (1) (2009) 67–74.
[33] C. Molinari, C. Zanelli, G. Guarini, M. Dondi, Bloating mechanism in lightweight aggregates: Effect of processing variables and properties of the vitreous phase, Constr. Build. Mater. 261 (2020), 119980.
[34] P. Billen, M. Mazzotti, L. Pandelaers, N. Ye oo, W. Zhao, Z. Liu, J. Redus, I. Diaz Loya, I. Bartoli, Y. Farnam, S. Spatari, Y.G. Hsuan, Melt ceramics from coal ash: Constitutive product design using thermal and flow properties, Resour. Conserv. Recycl. 132 (2018) 168–177.
[35] Y.M. Wie, K.G. Lee, K.H. Lee, Chemical design of lightweight aggregate to prevent adhesion at bloating activation temperature, J. Asian Ceram. Soc. 8 (2) (2020) 245–254.
[36] J.M. Moreno-Maroto, C.J. Cobo-Ceacero, M. Uceda-Rodríguez, T. Cotes-Palomino, C.M. García, J. Alonso-Azcárate, Unraveling the expansion mechanism in lightweight aggregates: Demonstrating that bloating barely requires gas, Constr. Build. Mater. 247 (2020), 118583.
[37] ASTM Subcommittee C09.20, C0127 - Standard Test Method for Relative Density (Specific Gravity) and Absorption of Coarse Aggregate, ASTM Int. (2015) 5. https://doi.org/10.1520/C0127-15.2.
[38] Standard Test Method for Relative Density (Specific Gravity) and Absorption of Fine Aggregate, ASTM Int. (2015).
[39] Standard Specification for Lightweight Aggregates for Structural Concrete, (n.d.).
[40] Standard Specification for Portland Cement, ASTM Int. (2105).
[41] C. ASTM, Standard practice for mechanical mixing of hydraulic cement pastes and mortars of plastic consistency, in: ASTM West Conshohocken, PA, 2014.
[42] J.R. Prestera, M. Boyle, D.A. Crocker, S.B. Chairman, E.A. Abdun-Nur, S.G. Barton, L.W. Bell, S.J. Blas Jr, G.R.U. Berg, P.M. Carrasquillo, Standard Practice for Selecting Proportions for Structural Lightweight Concrete (ACI 211.2-98), (1998).
[43] F. Althoey, Y. Farnam, Performance of calcium aluminate cementitious materials in the presence of sodium chloride, J. Mater. Civ. Eng. 32 (2020) 4020277.
[44] H.S. Esmaeeli, Y. Farnam, J.E. Haddock, P.D. Zavattieri, W.J. Weiss, Numerical analysis of the freeze-thaw performance of cementitious composites that contain phase change material (PCM), Mater. Des. 145 (2018) 74–87.
[45] Dragonfly, (2018). https://www.theobjects.com/dragonfly/index.html.
[46] Y. Shields, E. Garboczi, J. Weiss, Y. Farnam, Freeze-thaw crack determination in cementitious materials using 3D X-ray computed tomography and acoustic emission, Cem. Concr. Compos. 89 (2018) 120–129.
[47] M. Balapour, Characterizing Physical Properties of Lightweight Aggregate Made from Waste Coal Ash Using X-Ray Computed Tomography, (2020).
[48] A. Putz, J. Hinebaugh, M. Aghighi, H. Day, A. Bazylak, J.T. Gostick, Introducing OpenPNM: an open source pore network modeling software package, ECS Trans. 58 (2013) 79.
[49] J.T. Gostick, Versatile and efficient pore network extraction method using marker-based watershed segmentation, Phys. Rev. E. 96 (2017) 23307.
[50] Z.A. Khan, T. Tranter, M. Agnaou, A. Elkamel, J. Gostick, Dual network extraction algorithm to investigate multiple transport processes in porous materials: Image-based modeling of pore and grain scale processes, Comput. Chem. Eng. 123 (2019) 64–77.
[51] Tests for mechanical and physical properties of aggregates. Determination of compressibility and confined compressive strength of lightweight aggregates, Br. Stand. Doc. (2013).
[52] Y. Li, D. Wu, J. Zhang, L. Chang, D. Wu, Z. Fang, Y. Shi, Measurement and statistics of single pellet mechanical strength of differently shaped catalysts, Powder Technol. 113 (1-2) (2000) 176–184.
[53] S. Yashima, Y. Kanda, S. Sano, Relationships between particle size and fracture energy or impact velocity required to fracture as estimated from single particle crushing, Powder Technol. 51 (3) (1987) 277–282.
[54] Standard Test Method for Determining Density of Structural Lightweight Concrete, ASTM Int. (2019).
[55] Standard Specification for Flow Table for Use in Tests of Hydraulic Cement, ASTM Int. (2021).
[56] Standard Test Method for Compressive Strength of Cylindrical Concrete Specimens, ASTM Int. (2021).
[57] O. Linderoth, L. Wadsö, D. Jansen, Long-term cement hydration studies with isothermal calorimetry, Cem. Concr. Res. 141 (2021), 106344.
[58] .F.W. Taylor, Cement chemistry, Thomas Telford London, 1997.
[59] V. Cnudde, M.N. Boone, High-resolution X-ray computed tomography in geosciences: A review of the current technology and applications, Earth-Sci. Rev. 123 (2013) 1–17.
[60] ASTM, Standard Specification for Lightweight Aggregate for Internal Curing of Concrete, Aust N Z J Surg. 67 (1997) 664–666. https://doi.org/10.1520/C1761.
[61] R. Nemes, Z. Józsa, Strength of lightweight glass aggregate concrete, J. Mater. Civ. Eng. 18 (5) (2006) 710–714.
[62] J. Góra, W. Piasta, Impact of mechanical resistance of aggregate on properties of concrete, Case Stud. Constr. Mater. 13 (2020) e00438.
[63] M. Bernhardt, H. Tellesbø, H. Justnes, K. Wiik, Mechanical properties of lightweight aggregates, J. Eur. Ceram. Soc. 33 (13-14) (2013) 2731–2743.
[64] Y.C. Lim, S.-K. Lin, Y.-R. Ju, C.-H. Wu, Y.-L. Lin, C.-W. Chen, C.-D. Dong, Reutilization of dredged harbor sediment and steel slag by sintering as lightweight aggregate, Process Saf. Environ. Prot. 126 (2019) 287–296.
[65] A.P. Pagnoncelli, A. Tridello, D.S. Paolino, Modelling size effects for static strength of brittle materials, Mater. Des. 195 (2020), 109052.
[66] P. Monteiro, Concrete: Microstructure, Properties, and Materials, McGraw-Hill Publishing, 2006.
[67] B. Mota Gassó, Impact of alkali salts on the kinetics and microstructural development of cementitious systems, EPFL (2015).
[68] B. Mota, T. Matschei, K. Scrivener, Impact of NaOH and Na2SO4 on the kinetics and microstructural development of white cement hydration, Cem. Concr. Res. 108 (2018) 172–185.
[69] M. Balapour, Y. Farnam, Y.G. Hsuan, Method of Lightweight Aggregates Production from Waste-Coal Combustion Ash, (2021).